

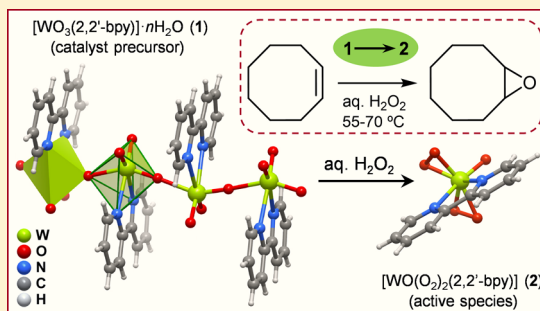
Crystal Structure and Catalytic Behavior in Olefin Epoxidation of a One-Dimensional Tungsten Oxide/Bipyridine Hybrid

Tatiana R. Amarante, Margarida M. Antunes, Anabela A. Valente,* Filipe A. Almeida Paz,* Martyn Pillinger, and Isabel S. Gonçalves*

Department of Chemistry, CICECO—Aveiro Institute of Materials, University of Aveiro, Campus Universitário de Santiago, 3810-193 Aveiro, Portugal

Supporting Information

ABSTRACT: The tungsten oxide/2,2'-bipyridine hybrid material $[\text{WO}_3(2,2'\text{-bpy})] \cdot n\text{H}_2\text{O}$ ($n = 1\text{--}2$) (**1**) has been prepared in near quantitative yield by the reaction of H_2WO_4 , 2,2'-bpy, and H_2O in the mole ratio of ca. 1:2:700 at 160 °C for 98 h in a rotating Teflon-lined digestion bomb. The solid-state structure of **1** was solved and refined through Rietveld analysis of high-resolution synchrotron X-ray diffraction data collected for the microcrystalline powder. The material, crystallizing in the orthorhombic space group *Iba*2, is composed of a one-dimensional organic–inorganic hybrid polymer, $\infty^1[\text{WO}_3(2,2'\text{-bpy})]$, topologically identical to that found in the previously reported anhydrous phases $[\text{MO}_3(2,2'\text{-bpy})]$ ($M = \text{Mo}, \text{W}$). While in the latter the *N,N'*-chelated 2,2'-bpy ligands of adjacent corner-shared $\{\text{MO}_4\text{N}_2\}$ octahedra are positioned on the same side of the 1D chain, in **1** the 2,2'-bpy ligands alternate above and below the chain. The catalytic behavior of compound **1** for the epoxidation of *cis*-cyclooctene was compared with that for several other tungsten- or molybdenum-based (pre)catalysts, including the hybrid polymer $[\text{MoO}_3(2,2'\text{-bpy})]$. While the latter exhibits superior performance when *tert*-butyl hydroperoxide (TBHP) is used as the oxidant, compound **1** is superior when aqueous hydrogen peroxide is used, allowing near-quantitative conversion of the olefin to the epoxide. With H_2O_2 , compounds **1** and $[\text{MoO}_3(2,2'\text{-bpy})]$ act as sources of soluble active species, namely, the oxidodiperoxo complex $[\text{MO}(\text{O}_2)_2(2,2'\text{-bpy})]$, which is formed in situ. Compounds **1** and $[\text{WO}(\text{O}_2)_2(2,2'\text{-bpy})]$ (**2**) were further tested in the epoxidation of cyclododecene, *trans*-2-octene, 1-octene, (*R*)-limonene, and styrene. The structure of **2** was determined by single-crystal X-ray diffraction and found to be isotypical with the molybdenum analogue.



INTRODUCTION

Metal oxide–organic hybrid materials have potential applications in many fields, such as catalysis, gas storage, electrical conductivity, magnetism, photochromism, and optics.^{1–3} Group VIb (Mo, W) systems are of particular interest, especially those in which N-donor molecules are directly coordinated to the oxide substructure.^{1,2} In an early report, layered molybdenum and tungsten trioxides were intercalated by pyridine (py) and 4,4'-bipyridine (4,4'-bpy) under strict anhydrous conditions to give the hybrid materials $[\text{MO}_3(\text{py})]$ ($M = \text{Mo}, \text{W}$) and $[\text{MoO}_3(4,4'\text{-bpy})_{0.5}]$, in which the heterocyclic nitrogen is directly coordinated to the metal atom of the oxide layer.⁴ The latter material was subsequently prepared by hydrothermal reaction of MoO_3 , 4,4'-bpy, and H_2O at 150 °C.⁵ Indeed, hydrothermal reactions of MO_3 (or simpler precursors like Na_2MO_4) with organonitrogen ligands, such as pyrazine (pyz),^{6–8} 2,2'-bpy and its derivatives,^{8–13} 4,4'-bpy,^{7,14} 1,10-phenanthroline,¹⁵ pyrazolylpyridines,¹⁶ 4,4'-bipyridylamine,¹⁷ and triazoles,^{5,18,19} have led to the isolation of a series of Mo (W) hybrid materials with structures based on one-dimensional (1D) chains, 2D networks, or 3D frameworks. Hydrolysis of dioxomolybdenum(VI) complexes of the type

$[\text{MoO}_2\text{Cl}_2(\text{L})]$ is an alternative route to such compounds.^{16,20,21} The catalytic potential of molybdenum(VI) oxide–organonitrogen systems for the epoxidation of olefins and the oxidation of secondary amines to nitrones has been studied.^{13,16,20–22} Depending on the structure and composition of the hybrid, as well as the catalytic reaction conditions, these materials act either as sources of soluble active species or as heterogeneous catalysts.

The structural inorganic chemistry of tungsten generally parallels that of molybdenum. Hence, several isotypical $\text{Mo}^{\text{VI}}/\text{W}^{\text{VI}}$ oxide–organonitrogen systems are known, such as $[\text{MO}_3(\text{py})]$,⁴ $[\text{MO}_3(\text{pyz})_{0.5}]$,^{6,7} $[\text{MO}_3(2,2'\text{-bpy})]$,^{9,10} and $[\text{MO}_3(4,4'\text{-bpy})_{0.5}]$.^{4,5,7} On the other hand, there are differences in the physicochemical properties of Mo^{VI} and W^{VI} (such as Pauling electronegativity, ionic radius, reduction potential, Lewis acid strength of the cations, and $\text{M}=\text{O}$ bond strengths), which can result in isotypical complexes or materials that exhibit contrasting behaviors for certain applications. Indeed, tungsten oxide-based materials, including inorganic–organic

Received: April 27, 2015

hybrids, have attracted increasing interest because of their unique properties and corresponding applications in optics and electronics.^{8,23–25} For example, Tallon and co-workers doped the layered hybrid material $[\text{WO}_3(4,4'\text{-bpy})_{0.5}]$ with Na^+ , K^+ , and Ca^{2+} ions so as to alter the electronic structure and increase conductivity.^{23–25} Such materials may also exhibit unique catalytic properties, taking into account the contrasting behaviors often encountered for molecular $\text{Mo}^{\text{VI}}/\text{W}^{\text{VI}}$ catalysts.^{26–30} In catalytic olefin epoxidation, for example, W-based catalysts usually show a lower activity than Mo-based catalysts in the presence of *tert*-butyl hydroperoxide (TBHP) as the oxidant. However, the situation is often reversed when H_2O_2 is the oxidant, with the W-based catalysts being superior.^{28–30} These differences may be due to a complex interplay of various factors, such as different inhibiting effects of water (much stronger for Mo than for W), greater oxophilicity, and Lewis acidity of the W^{VI} center.³⁰

Inspired by our successful investigations into molybdenum oxide–organonitrogen systems as catalysts or catalyst precursors for oxidation reactions, we have started to explore tungsten oxide systems. An additional motivation for such studies is the above-mentioned tendency for oxotungsten(VI) catalysts to work well with aqueous H_2O_2 , which is recognized as a cheap, safe, and environmentally clean oxidant. Here, we report the first account of the catalytic behavior of a tungsten oxide–organonitrogen hybrid material, namely, $[\text{WO}_3(2,2'\text{-bpy})] \cdot n\text{H}_2\text{O}$. The epoxidation of *cis*-cyclooctene has been chosen as a model reaction, using TBHP or H_2O_2 as oxidant, and emphasis has been placed on studying the stability of the hybrid and identifying the nature of the catalytically active species. In addition, the structure of the hybrid has been solved and refined through Rietveld analysis of high-resolution synchrotron X-ray diffraction data.

EXPERIMENTAL SECTION

Materials and Methods. For synthesis, H_2WO_4 (puriss p.a., Fluka), 2,2'-bipyridine (98.0%, Fluka), acetonitrile (analytical reagent, Lab-Scan), and diethyl ether (puriss p.a., Sigma-Aldrich) were acquired from commercial sources and used as received. The material $[\text{MoO}_3(2,2'\text{-bpy})]$ was prepared as described previously.³¹ For the catalytic experiments, the olefins *cis*-cyclooctene (95%), cyclododecene (96%, mixture *cis/trans*), *trans*-2-octene (97%), 1-octene, (*R*)-limonene (97%), and styrene (99%) were obtained from Sigma-Aldrich and used as received. 1,2-Dichloroethane (99%, Aldrich), ethanol (>99.9% analytical grade, Scharlau ACS), anhydrous α,α,α -trifluorotoluene ($\geq 99\%$, Sigma-Aldrich), acetonitrile ($\geq 99\%$, Aldrich), undecane (99%, Sigma-Aldrich), 5.5 M *tert*-butyl hydroperoxide in decane (Sigma-Aldrich), 70% aq *tert*-butyl hydroperoxide (Aldrich), and 30% aq H_2O_2 (Riedel-de Haën) were acquired from commercial sources and used as received.

Elemental analysis for C, H, and N was performed at the University of Aveiro with a Leco TruSpec 630-200-200 analyzer. Routine powder X-ray diffraction (PXRD) data were collected at ambient temperature on a Philips Analytical Empyrean ($\theta/2\theta$) diffractometer equipped with a PIXcelID detector, with automatic data acquisition (X'Pert Data Collector software v4.2) using monochromatized $\text{Cu K}\alpha$ radiation ($\lambda = 1.5406 \text{ \AA}$). Intensity data were collected by the step-counting method (step 0.01°), in continuous mode, in the ca. $3.5^\circ \leq 2\theta \leq 50^\circ$ range. Scanning electron microscopy (SEM) images were collected using a Hitachi SU-70 microscope operating at 20 kV. Samples were prepared by deposition on aluminum sample holders followed by carbon coating using an Emitech K 950 carbon evaporator. Thermogravimetric analysis (TGA) was carried out using a Shimadzu TGA-50 instrument, from ambient temperature to ca. 800°C , under a continuous stream of air at a flow rate of 20 mL min^{-1} and a heating rate of 5°C min^{-1} .

FT-IR spectra were collected using KBr (Sigma-Aldrich, 99%, FT-IR grade) pellets and a Mattson-7000 infrared spectrophotometer. Attenuated total reflectance (ATR) FT-IR spectra were measured using a Specac Golden Gate Mk II ATR accessory having a diamond top plate and KRS-5 focusing lenses. Solid-state ^{13}C cross-polarization (CP) magic-angle-spinning (MAS) NMR spectra were recorded using a Bruker Avance 400 spectrometer (9.4 T) at 100.62 MHz with $3.7 \mu\text{s}$ ^1H 90° pulses, 1.5 ms contact time, spinning rates of 10–12 kHz, and 5 s recycle delays. Chemical shifts are quoted in parts per million (ppm) from tetramethylsilane.

$[\text{WO}_3(2,2'\text{-bpy})] \cdot n\text{H}_2\text{O}$ (**1**). A mixture of H_2WO_4 (0.49 g, 1.96 mmol), 2,2'-bpy (0.62 g, 3.97 mmol), and H_2O (25 mL) was heated in a rotating (15 rpm) Teflon-lined stainless steel digestion bomb at 160°C for 98 h. After cooling down to ambient temperature, the resultant microcrystalline white solid was separated from the pink aqueous liquor (pH 6) by filtration, washed with an excess of water and diethyl ether ($4 \times 10 \text{ mL}$), and finally dried at 80°C . Yield: 0.80 g, 96% (based on W). Anal. Calcd for $\text{C}_{10}\text{H}_{12}\text{N}_2\text{O}_5\text{W}$ ($[\text{WO}_3(2,2'\text{-bpy})] \cdot 2\text{H}_2\text{O}$): C, 28.32; H, 2.85; N, 6.61. Found: C, 28.30; H, 2.63; N, 6.63. TGA showed a weight loss of 6.7% up to 150°C (calcd: for loss of $2\text{H}_2\text{O}$, 8.5%; for loss of $1.5\text{H}_2\text{O}$, 6.5%). Selected FT-IR (KBr, cm^{-1}): $\nu = 3397$ (s, br), 3313 (s, br), 3112 (m), 3079 (m), 3035 (m), 1650 (m), 1600 (s), 1575 (w), 1567 (w), 1540 (vw), 1494 (m), 1475 (m), 1446 (s), 1313 (m), 1170 (m), 1160 (w), 1122 (w), 1029 (m), 979 (w), 939 (m), 883 (vs), 846 (s), 775 (vs), 655 (vs), 455 (m), 435 (w), 414 (m), 372 (m), 349 (s). $^{13}\text{C}\{^1\text{H}\}$ CP MAS NMR: $\delta = 123.8, 124.5, 125.7$ (C3/C3', C5/C5'), 138.8, 142.4 (C4/C4'), 148.4 (C6/C6'), 149.6, 150.6 (C2/C2') ppm.

$[\text{WO}(\text{O}_2)_2(2,2'\text{-bpy})]$ (**2**). A mixture comprising $[\text{WO}_3(2,2'\text{-bpy})] \cdot n\text{H}_2\text{O}$ (0.25 g, 0.59 mmol with $n = 2$), 30% aq H_2O_2 (10.2 mL, 0.09 mol), and CH_3CN (65 mL) was heated at 70°C for 24 h. The resultant white precipitate was separated by filtration, washed with cold distilled water and ethanol, and finally vacuum-dried at ambient temperature. Yield: 0.16 g, 65%. Anal. Calcd for $\text{C}_{10}\text{H}_8\text{N}_2\text{O}_5\text{W}$: C, 28.59; H, 1.92; N, 6.67. Found: C, 28.40; H, 2.01; N, 6.61. Selected FT-IR (KBr, cm^{-1}): $\nu = 3448$ (vs, br), 3112 (m), 3085 (s), 1637 (w), 1608 (sh), 1600 (s), 1571 (m), 1560 (m), 1496 (m), 1473 (s), 1446 (s), 1423 (m), 1315 (m), 1243 (m), 1220 (w), 1176 (m), 1160 (m), 1047 (m), 1035 (m), 1022 (w), 944 (vs), 847 (sh), 835 (s), 775 (s), 728 (m), 665 (m), 649 (m), 595 (m), 541 (s), 416 (w). $^{13}\text{C}\{^1\text{H}\}$ CP MAS NMR: $\delta = 122.1, 123.3, 125.4, 128.7$ (C3/C3', C5/C5'), 144.0, 146.7 (C4/C4'), 147.9, 149.5 (C6/C6'), 153.9, 155.4 (C2/C2') ppm.

Crystals suitable for X-ray diffraction were obtained by slow evaporation of the filtrate from the above reaction. The PXRD pattern of the bulk product **2** was in excellent agreement with a simulated pattern calculated from the single-crystal X-ray structural data (Figure S1 in the Supporting Information).

X-ray Diffraction Studies. The structures of **1** and **2** were determined by powder and single-crystal XRD, respectively. High-resolution PXRD data suitable for crystal solution were collected at 100 K on the powder diffractometer at the ID22 beamline of the European Synchrotron Radiation Facility (ESRF), Grenoble, France. Tables 1 and 2 gather all the details pertaining to the X-ray data collection, crystal data, and structure refinement for **1** and **2**. The final Rietveld plot for **1** is supplied in Figure 1. A complete description of the procedures used in the powder and single-crystal XRD studies is given in the Supporting Information. Structural drawings were created using the software package Crystal Impact Diamond.³³

Catalytic Tests. The catalytic tests were carried out at 55 or 70°C under air in closed borosilicate batch reactors (5 mL capacity) equipped with a magnetic stirrer (1000 rpm) and a valve for sampling. Typically, the reaction vessel was loaded with **1**, **2**, or $[\text{MoO}_3(2,2'\text{-bpy})]$ (0.018 mmol); olefin (1.8 mmol); oxidant (3 mmol); and cosolvent (2 mL, when applied). The cosolvent was either 1,2-dichloroethane (DCE), ethanol (EtOH), α,α,α -trifluorotoluene (TFT), or acetonitrile (CH_3CN). The oxidant solution was 70% aq *tert*-butyl hydroperoxide (TBHP_{aq}), 5.5 M *tert*-butyl hydroperoxide in decane (TBHP_{dec}), or 30% aq H_2O_2 . The reactor containing $[\text{MO}_3(2,2'\text{-bpy})]$ ($M = \text{Mo}, \text{W}$) or $[\text{WO}(\text{O}_2)_2(2,2'\text{-bpy})]$, olefin, and cosolvent (when applied) was preheated at the desired reaction

Table 1. X-ray Data Collection, Crystal Data, and Structure Refinement Details for [WO₃(2,2'-bpy)]·nH₂O (1)

data collection	
diffractometer	ID22 beamline, ESRF, France
wavelength (Å)	0.495958(7)
temp (K)	100
geometry	Debye–Scherrer
2θ range (deg)	1.002–30.000
unit cell	
formula	C ₁₀ H ₈ N ₂ O ₄ W ^b
crystal system	orthorhombic
space group	Iba2
a (Å)	19.03471(18)
b (Å)	17.14447(16)
c (Å)	7.27897(4)
volume (Å ³)	2375.42(3)
Z	8
D _c (g cm ⁻³)	2.259(1)
Profile Parameters	
profile function	fundamental parameters approach
zero shift (2θ°)	0.003(1)
Refinement Details	
no. of independent reflections	817
no. of global refined parameters	102
R _p , R _{wp} , R _{exp} , GOF ^a	9.44, 13.16, 0.91, 14.5
Structure Reliability Factors	
R _{Bragg} ^a	5.40

^aR_p = $\sum_i |y_{i,o} - y_{i,c}| / \sum_i |y_{i,o}|$, R_{wp} = $[\sum_i w_i (y_{i,o} - y_{i,c})^2 / \sum_i w_i y_{i,o}^2]^{1/2}$, R_{Bragg} = $\sum_m |I_{n,o} - I_{n,c}| / \sum_m I_{n,o}$, R_{exp} = $[(n - p) / \sum_i w_i y_{i,o}^2]^{1/2}$, GOF = R_{wp} / R_{exp}, where y_{i,o} and y_{i,c} are the observed and calculated profile intensities and I_{n,o} and I_{n,c} are the observed and calculated intensities, respectively. The summations run over *i* data points or *n* independent reflections. Statistical weights w_i are usually taken as 1/y_{i,o}. ^bHydrogen atoms from the water molecule of crystallization have not been included.

temperature for 10 min, and afterward, the oxidant solution (also preheated in the case of TBHP) was added to the reactor; the reaction time was counted from this instant. The catalytic reactions were monitored using a Varian 3800 GC equipped with a capillary column (DB-5, 30 m × 0.25 mm) and a flame ionization detector. The reaction products were identified by GC–MS (Trace GC 2000 Series (Thermo Quest CE Instruments)-DSQ II (Thermo Scientific) equipped with a capillary column (DB-5 MS, 30 m × 0.25 mm × 0.25 μm), using He as carrier gas).

After each 24 h batch run (with EtOH as cosolvent), a solid was separated by centrifugation at 3500 rpm, thoroughly washed with ethanol, and dried overnight at ambient temperature and then under vacuum for 1 h at 65 °C. The recovered solids were reused in consecutive 24 h batch runs using similar initial mass ratios of olefin:oxidant:catalyst:cosolvent to those used in the first run.

Contact tests (CTs) were carried out for **1** (with EtOH or CH₃CN as cosolvent) in order to assess whether the catalytic reaction was homogeneous or heterogeneous. The CTs consisted of treating **1** under typical reaction conditions, but without the substrate, for 24 h at 70 °C. Subsequently, the (undissolved) solid was separated by centrifugation, washed, and dried overnight at ambient temperature and then under vacuum for 1 h at 65 °C, giving sol-CT-EtOH and sol-CT-CH₃CN. The solution obtained from the CT was passed through a syringe equipped with a 0.2 μm VWR nylon membrane filter, giving liq-CT-EtOH and liq-CT-CH₃CN. The solids and solutions obtained from the CTs were tested in the reaction of Cy under typical conditions, at 70 °C.

Table 2. Crystal and Structure Refinement Data for Compound [WO(O₂)₂(2,2'-bpy)] (2)

formula	C ₁₀ H ₈ N ₂ O ₃ W
formula weight	420.03
crystal system	monoclinic
space group	P2 ₁ /n
a (Å)	6.2509(6)
b (Å)	12.5514(11)
c (Å)	13.6903(12)
β (deg)	91.851(3)
volume (Å ³)	1073.55(17)
Z	4
D _c (g cm ⁻³)	2.599
μ(Mo Kα) (mm ⁻¹)	10.776
crystal size (mm)	0.22 × 0.06 × 0.04
crystal type	colorless needles
θ range	3.54–25.34
index ranges	−7 ≤ h ≤ 7, −15 ≤ k ≤ 15, −16 ≤ l ≤ 16
reflections collected	14503
independent reflections	1967 [R _{int} = 0.0694]
completeness to θ = 25.24°	99.8%
final R indices [I > 2σ(I)] ^{a,b}	R1 = 0.0316, wR2 = 0.0585
final R indices (all data) ^{a,b}	R1 = 0.0460, wR2 = 0.0623
weighting scheme ^c	m = 0.0054, n = 10.1229
largest diff. peak and hole	1.941 and −1.097 e Å ⁻³

^aR1 = $\sum ||F_o| - |F_c|| / \sum |F_o|$, ^bwR2 = $(\sum [w(F_o^2 - F_c^2)^2] / \sum [w(F_o^2)^2])^{1/2}$. ^cw = $1 / [\sigma^2(F_o^2) + (mP)^2 + nP]$, where P = $(F_o^2 + 2F_c^2) / 3$.

RESULTS AND DISCUSSION

Synthesis and Physicochemical Characterization of [WO₃(2,2'-bpy)]·nH₂O (n = 1–2) (1). Compound **1** was obtained in excellent yield (96%) by the reaction of H₂WO₄, 2,2'-bpy, and H₂O in the mole ratio of ca. 1:2:700 at 160 °C for 98 h in a Teflon-lined digestion bomb. Previously, Twu et al. reported the isolation of [WO₃(2,2'-bpy)] in 80% yield, using exactly the same starting materials, reaction temperature, and time.¹⁰ The higher yield obtained in the present work may be because we performed the hydrothermal synthesis with continuous rotation of the bomb, while Twu et al. apparently carried out the reaction under static conditions. As will be described below, performing the synthesis under dynamic conditions leads not only to a higher yield but also to a unique structure for the 1D ∞¹[WO₃(2,2'-bpy)] polymer present in the crystal structure of **1**.

Compound **1** was characterized by elemental analysis, TGA, FT-IR spectroscopy, ¹³C{¹H} MAS NMR, and PXRD, including a complete structural determination using synchrotron X-ray data (described below). TGA of **1** revealed a weight loss of 6.7% between ambient temperature and 150 °C, with a plateau being reached at 100 °C (Figure S2 in the Supporting Information), assigned to the removal of water molecules of crystallization and residual physisorbed water (1–2 water molecules per formula unit). In contrast, the tungsten oxide/bipyridine hybrid material reported by Twu et al. was found to be anhydrous.¹⁰ On the other hand, the two materials present similar thermal behavior above 150 °C, with decomposition taking place between 200 and 450 °C. For compound **1**, three overlapping steps contribute to a net weight loss of 37.0%. The residual mass of 55.9% at 450 °C is in excellent agreement with the theoretical value of 55.9%, calculated assuming loss of 2,2'-

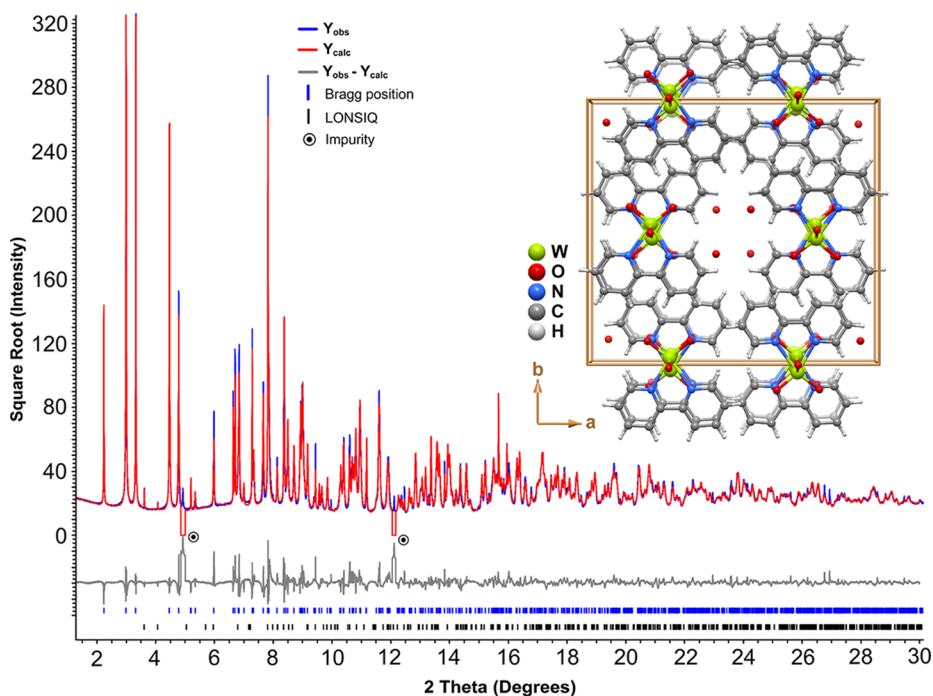


Figure 1. Final Rietveld plot of $[\text{WO}_3(2,2'\text{-bpy})]\cdot n\text{H}_2\text{O}$ (**1**) ($n = 1$). Observed data points are indicated as a blue line, the best fit profile (upper trace) and the difference pattern (lower trace) are drawn as solid red and gray lines, respectively. Blue and gray vertical bars indicate the angular positions of the allowed Bragg reflections for **1** and the reported analogous compound with CCDC refcode LONSIQ, respectively.³² Relative amounts (wt %) of the two samples present in the bulk material are 99.88(1):0.12(1) (**1**:LONSIQ). Refinement details are given in Table 1. The inset depicts a perspective view along the [001] direction of the unit cell of **1**.

bpy and formation of WO_3 , with $n = 1.5$ (water content) in the starting material. SEM of **1** showed that the morphology consists of long, thin needles (Figure 2).

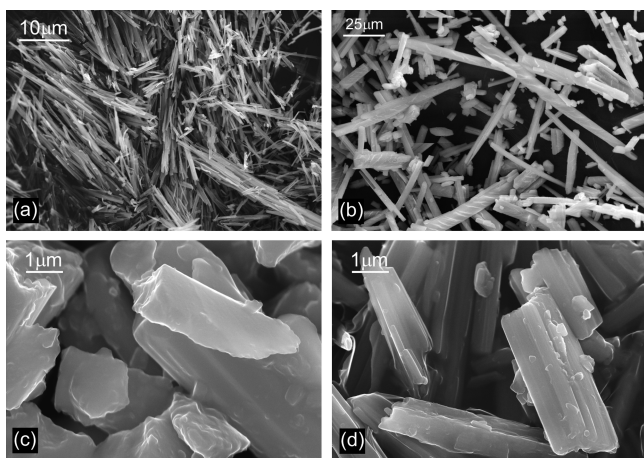


Figure 2. Representative SEM images of (a) **1**, (b) **2**, and the solids recovered after the (c) first (CH_3CN as cosolvent) and (d) second (EtOH as cosolvent) catalytic runs, with **1** as (pre)catalyst.

In the range of $500\text{--}950\text{ cm}^{-1}$, the FT-IR spectrum of **1** displays sharp bands at 775 , 846 , 883 , and 939 cm^{-1} and a broad, very intense absorption at 655 cm^{-1} , similar to the data published by Twu et al. for $[\text{WO}_3(2,2'\text{-bpy})]$.¹⁰ The band at 775 cm^{-1} is assigned as a ligand ($2,2'\text{-bpy}$) mode, while the other bands are assigned as $\text{W}\text{--}\text{O}$ vibrations ($\nu_{\text{W}=\text{O}}$ between 840 and 940 cm^{-1} and $\nu_{\text{W}\text{--}\text{O}\text{--}\text{W}}$ at 655 cm^{-1}). The molybdenum analogue, $[\text{MoO}_3(2,2'\text{-bpy})]$, exhibits a similar set of bands at 622 , 760 , 882 , and 914 cm^{-1} .^{20,31} The $^{13}\text{C}\{^1\text{H}\}$

CP MAS NMR spectrum of **1** displays eight separate signals in the range of $120\text{--}150\text{ ppm}$, suggesting that the two pyridyl groups of the ligand are not equivalent in the crystal structure of **1** (Figure 3). Indeed, the two signals at 123.8 and 148.4 ppm are slightly broader than the remaining resonances; hence, each of these two signals probably comprises two overlapping

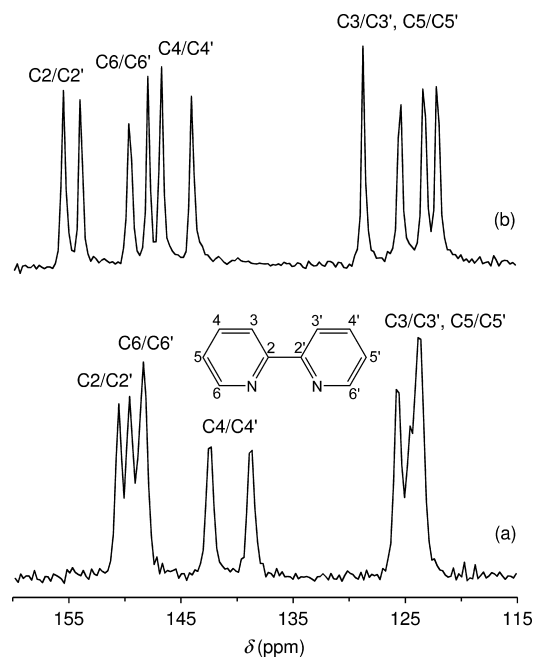


Figure 3. $^{13}\text{C}\{^1\text{H}\}$ CP MAS NMR spectra of (a) the hybrid **1** and (b) the oxodiperoxo complex **2**.

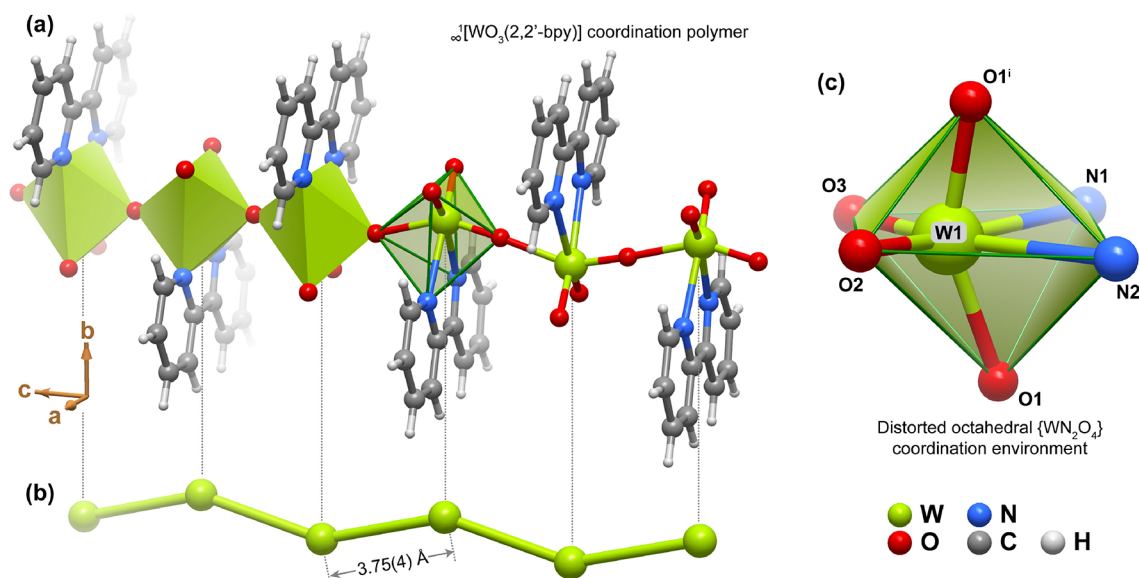


Figure 4. Schematic representation of the (a) 1D, neutral $\infty^1[\text{WO}_3(2,2'\text{-bpy})]$ polymer present in the crystal structure of **1** running parallel to the *c*-axis, emphasizing the (b) zigzag nature of the polymer and the intermetallic distance. (c) Distorted octahedral coordination environment of the crystallographically unique W^{VI} center. Symmetry transformation used to generate equivalent atoms: (i) $-x, 1 - y, -1 + z$.

resonances (for C3/C3' or C5/C5', and C6/C6', respectively), giving the expected total of ten resonances.

High-Resolution Powder Synchrotron XRD Studies of $[\text{WO}_3(2,2'\text{-bpy})]\cdot n\text{H}_2\text{O}$ (1**).** The main crystalline product obtained from the hydrothermal reaction of tungstic acid with 2,2'-bpy was formulated as $[\text{WO}_3(2,2'\text{-bpy})]\cdot n\text{H}_2\text{O}$ on the basis of high-resolution PXRD data ($n = 1$). As clearly observed in the collected powder pattern, the material has trace amounts of crystalline impurities (Figure 1). One of these impurities was unequivocally identified as the related $[\text{WO}_3(2,2'\text{-bpy})]$ phase reported by Yan et al. (CCDC refcode LONSIQ), single-crystals of which were obtained by the hydrothermal reaction of Na_2WO_4 , 2,2'-bpy, and H_2O at 190°C .³² The LONSIQ phase, which is isotypical with the corresponding molybdenum compound reported by Zubieta and co-workers,⁹ was obtained in a microcrystalline form by Twu et al.¹⁰ as described above. A second impurity (highlighted in Figure 1) has not yet been identified, but it does not correspond to any of the starting materials used in the synthesis or possible secondary products the crystalline structure of which has been reported and deposited in the Cambridge Structural Database. Rietveld analysis assuming solely a mixture of **1** with LONSIQ (the section of the powder pattern affected by the second impurity was masked) clearly showed that the latter material is present in trace amounts, accounting for only 0.12(1)% by weight of the total sample (a value typically smaller than ca. 5% may be considered as negligible).

The main structural feature of **1** concerns the presence of a 1D, neutral $\infty^1[\text{WO}_3(2,2'\text{-bpy})]$ hybrid polymer (Figure 4a). The basic building unit of this polymer is a six-coordinated W^{VI} metal center bonded to three oxo groups (two terminal and one μ_2 -bridging) and one *N,N'*-chelated 2,2'-bpy organic moiety. The coordination geometry of the resulting $\{\text{WN}_2\text{O}_4\}$ polyhedron resembles a highly distorted octahedron (Figure 4c). Although the polymer in **1** is topologically identical to that reported by Yan et al.,³² there is a marked distinction concerning the orientation of the 2,2'-bpy organic ligands. In the compound reported herein, the *N,N'*-chelated 2,2'-bpy moieties of adjacent coordination polyhedra alternate below

and above the growth axis of the inorganic core of the polymer (the torsion angle between consecutive moieties is ca. 175°), being mutually placed in approximately parallel planes (Figure 5b). This behavior for organic linkers was previously reported for the secondary $[\text{WO}_3(\text{en})]$ phase described by Yang et al.,³⁴ where en = ethylenediamine. Conversely, in the structure reported by Yan et al.,³² the 2,2'-bpy ligands are on the same side of the inorganic core of the chain, being slightly tilted along that direction (the torsion angle between adjacent ligands is ca. 50°). As shown in Figure 5a, consecutive 2,2'-bpy ligands in LONSIQ are placed on average planes that subtend a mutual dihedral angle of ca. 11.5° . Figure 5c overlays the two topologically identical, but conformationally distinct, $\infty^1[\text{WO}_3(2,2'\text{-bpy})]$ polymers present in **1** and LONSIQ, emphasizing the geometrical differences described above.

The presence of distinct chemical moieties in the $\{\text{WN}_2\text{O}_4\}$ coordination polyhedron and the marked trans effect of the terminal oxo groups contribute to the highly distorted coordination geometry observed in **1**: while the $\text{W}-(\text{N},\text{O})$ bond distances range from 1.755(16) to 2.334(7) Å, the cis and trans $(\text{N},\text{O})-\text{W}-(\text{N},\text{O})$ octahedral internal angles fall within the ranges of $71.45(15)^\circ$ – $110.9(17)^\circ$ and $153(2)^\circ$ – $164.4(5)^\circ$, respectively (Table 3). These values are in very good agreement with the geometrical data reported by Yan et al. for LONSIQ, with the corresponding intervals being 1.714(9)–2.381(11) Å, $68.8(4)^\circ$ – $107.0(5)^\circ$, and $150.7(4)^\circ$ – $163.4(4)^\circ$.³² To further compare these two structures and to evaluate any variation in the degree of distortion of the W^{VI} octahedra between **1** and LONSIQ, an adaptation of the mathematical method proposed by Baur³⁵ was employed to calculate a distortion index (DI) for bonds and angles:

$$\text{DI}_{\text{Bond}} = \frac{\sum_{i=1}^n |d(\text{W}-(\text{N},\text{O}))_i - d(\text{W}-(\text{N},\text{O}))_{\text{average}}|}{\sum_{i=1}^n |d(\text{W}-(\text{N},\text{O}))_i|} \quad (1)$$

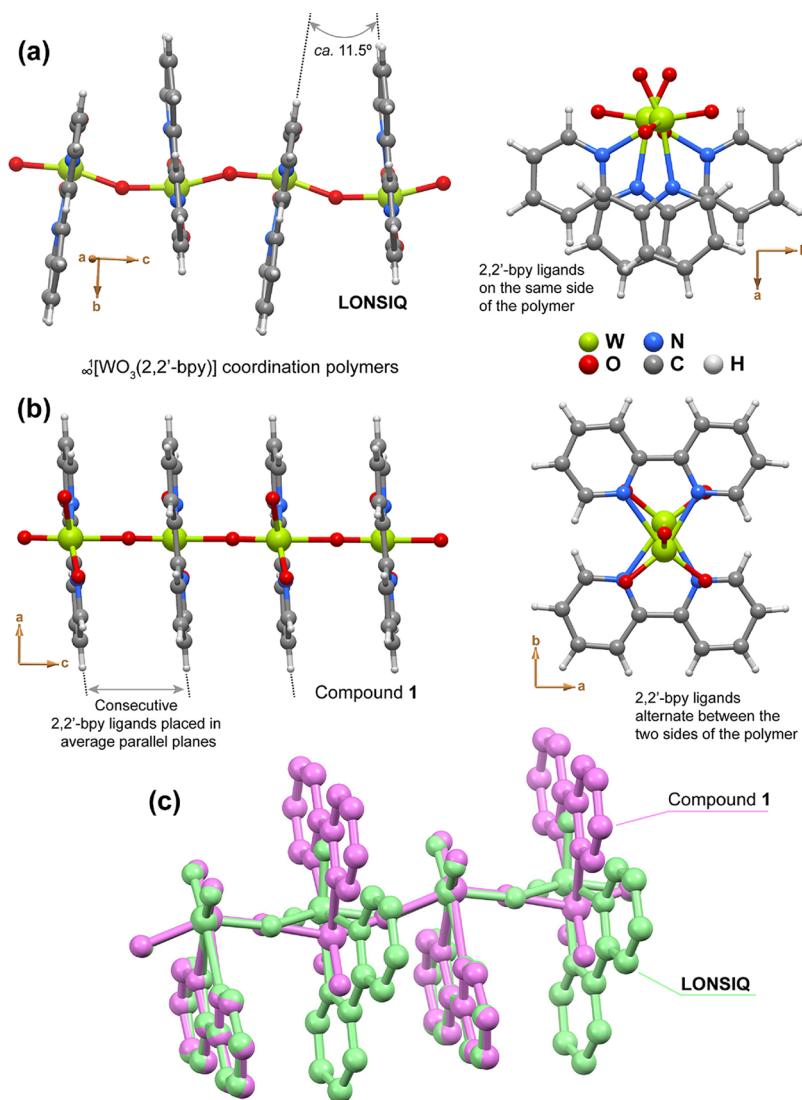


Figure 5. Comparison between the geometrical features of the 1D, neutral $\infty^1[\text{WO}_3(2,2'\text{-bpy})]$ polymers present in compound 1 and in the crystal structure reported by Yan et al.³² (CCDC refcode LONSIQ).

Table 3. Selected Bond Lengths (Å) and Angles (deg) for the Crystallographically Independent W^{VI} Center Present in $[\text{WO}_3(2,2'\text{-bpy})] \cdot n\text{H}_2\text{O}$ (1) ($n = 1$)^a

W1–O1	1.99(6)	O1–W1–O1 ⁱ	153(2)
W1–O1 ⁱ	1.78(6)	O1–W1–O2	110.9(17)
W1–O2	1.84(2)	O1 ⁱ –W1–O2	83.5(18)
W1–O3	1.755(16)	O1–W1–O3	99(2)
W1–N1	2.323(3)	O1 ⁱ –W1–O3	100(2)
W1–N2	2.334(7)	O1 ⁱ –W1–N1	85.5(15)
		O1 ⁱ –W1–N2	78.2(19)
		O1–W1–N1	74.2(13)
		O1–W1–N2	77.8(17)
		O2–W1–O3	102.5(8)
		O2–W1–N1	162.4(11)
		O2–W1–N2	92.8(6)
		O3–W1–N1	93.0(5)
		O3–W1–N2	164.4(5)
		N1–W1–N2	71.45(15)

^aSymmetry transformation used to generate equivalent atoms: (i) $-x$, $1 - y$, $-1 + z$.

$$DI_{\text{Angle}} = \frac{\sum_{i=1}^n |((\text{N},\text{O})-\text{W}-(\text{N},\text{O}))_i - ((\text{N},\text{O})-\text{W}-(\text{N},\text{O}))_{\text{ideal}}|}{\sum_{i=1}^n |((\text{N},\text{O})-\text{W}-(\text{N},\text{O}))_i|} \quad (2)$$

where the subscripts i and average/ideal correspond to individual and average/ideal bond lengths and angles (see Table 3 for individual data). The DI_{Bond} values for the W^{VI} centers are 0.11 and 0.12 for 1 and LONSIQ, respectively, while the DI_{Angle} values for the cis/trans angles are 0.12/0.13 for 1 and 0.12/0.14 for LONSIQ. These results clearly demonstrate that the rotation of the N,N' -chelated 2,2'-bpy organic linkers along the $\text{W} \rightarrow \mu_2\text{-O} \rightarrow \text{W}$ direction of the inorganic backbone of the polymer does not significantly affect the geometry of the $\{\text{WN}_2\text{O}_4\}$ coordination polyhedron, which is equally highly distorted in both compounds.

One main difference observed for the $\infty^1[\text{WO}_3(2,2'\text{-bpy})]$ polymers present in 1 and LONSIQ resides in the intermetallic $\text{W} \cdots \text{W}$ distance along the $\text{W} \rightarrow \mu_2\text{-O} \rightarrow \text{W}$ direction of the polymer. While in LONSIQ this distance is 3.6766(8) Å, in 1 the distance is slightly longer, being 3.75(4) Å (Figure 4b). The

“kink” ($W-(\mu_2-O)-W$) angle is also higher in the structure of **1** [$171(3)^\circ$ versus $147.7(5)^\circ$ for LONSIQ]. These distinct structural features seem to mostly arise from the orientation of the pendant N,N' -chelated ligands, which influences the supramolecular contacts present in the structure (see below). Similarly, in the $[WO_3(en)]$ structure described by Yang et al.,³⁴ in which the ligands alternate above and below the growth direction of the polymer, the intermetallic $W\cdots W$ distance is greater [$3.7247(8)$ Å] than in LONSIQ, with a $W-(\mu_2-O)-W$ angle of $152.3(11)^\circ$.

Compound **1** contains one water molecule of crystallization per W^{VI} center, while LONSIQ is completely anhydrous. Because of the strong hydrophobic nature of the organic ligand, these water molecules are engaged in mostly weak supramolecular contacts in the crystal structure. Even though the alternate rotation of the 2,2'-bpy organic ligands along the growth direction of the polymer gives rise to 1D channels in which these water molecules reside, their inclusion may not be the reason for the different conformations observed for **1** and LONSIQ. Indeed, in the $[WO_3(en)]$ crystal structure, the en ligands adopt the same alternate orientation and the structure does not include any solvent molecules. Hence, the presence of water molecules in the crystal structure of **1** probably results from the need to essentially fill the available space, not being a crucial and directing structural feature. Under the high-energy X-ray beam of the synchrotron, these molecules may be easily removed (even at low temperatures), thus promoting the formation of partially dehydrated phases that could account for the small amount of crystalline impurities.

The crystal packing of **1** (inset in Figure 1) is essentially mediated by the need to effectively fill the available space alongside with a number of cooperative, weak $C-H\cdots O$ hydrogen-bonding interactions. The most notable ones concern the interactions along the b -axis interconnecting adjacent $\infty^1[WO_3(2,2'-bpy)]$ polymers, in which the N,N' -chelated 2,2'-bpy molecule from one chain interacts with the two terminal oxo groups of the neighboring one (see Figure S3a of the Supporting Information). These interactions are, in general, highly directional (at least two with interactions angles close to ca. 180° ; see Table S1, Supporting Information), ultimately contributing to a strong cohesion of the polymers in the solid state. These interpolymer connections are reinforced by the $C4-H14\cdots O3$ hydrogen-bonding connection along the $[001]$ direction of the unit cell (Figure S3b, Supporting Information). The water molecules of crystallization lie, as mentioned above, in the channels of the structure and interact weakly with neighboring N,N' -chelated 2,2'-bpy molecules (Figure S4, Supporting Information). Even though the $\angle(DHA)$ interaction angles are typically greater than ca. 160° , the interatomic distance between donor and acceptors are relatively long (usually greater than ca. 3.4 Å; see Table S1, Supporting Information).

Catalytic Epoxidation of *cis*-Cyclooctene. Effect of Oxidant, Cosolvent, and Temperature and Comparison with Literature Data. Compound **1** was explored as a (pre)catalyst for olefin epoxidation using *cis*-cyclooctene (Cy) as a benchmark substrate. First, $TBHP_{dec}$ was used as oxidant, no cosolvent was added, and the reaction was performed at $55^\circ C$. Excellent selectivity (100%) toward cyclooctene oxide (CyO) was observed for **1**, but the catalytic activity was very poor (10% conversion at 24 h reaction, Table 4). As mentioned in the introduction, poor catalytic results are frequently reported in the literature for tungsten compounds tested as

Table 4. Influence of the Reaction Conditions on the Epoxidation of *cis*-Cyclooctene in the Presence of **1^a**

oxidant	cosolvent	temp ($^\circ C$)	conversion (%)	CyO selectivity (%)	
$TBHP_{dec}$	none	55	10	100	
	none	70	57	100	
	DCE	70	4	100	
	TFT	70	4	100	
	EtOH	70	1	100	
$TBHP_{aq}$	CH_3CN	70	8	100	
	CH_3CN	70	2	100	
	H_2O_2	CH_3CN	55	77	100
	H_2O_2	CH_3CN	70	98	100
	H_2O_2	EtOH	70	99	100

^aReaction conditions: initial molar ratios of $W: Cy: oxidant = 1:100:167$, 2 mL of cosolvent (when applied), 24 h.

(pre)catalysts in the same reaction, e.g., cyclopentadienyl compounds of the type $[Cp'W(CO)_3R]$ (Table 5).³⁶

For **1**, increasing the reaction temperature from 55 to $70^\circ C$ enhanced the reaction rate (57% conversion at 24 h) without affecting epoxide selectivity, which was always 100% (Table 4, Figure 6). At this higher reaction temperature, the addition of a cosolvent (DCE, TFT, EtOH, or CH_3CN) had a detrimental effect, with CyO yields at 24 h being in the range of 1–8%, similar to the 2% conversion observed without catalyst. In contrast, the molybdenum analogue $[MoO_3(2,2'-bpy)]$ exhibits much higher activity when used as the catalyst for the same reaction with $TBHP_{dec}$ as oxidant and DCE as cosolvent: 95% conversion at 6 h/ $55^\circ C$ and 100% conversion at 1 h/ $75^\circ C$.³¹ In the presence of **1**, the reaction of Cy was sluggish for both the organic ($TBHP_{dec}$) and aqueous ($TBHP_{aq}$) solutions of TBHP. The reaction mixtures were always biphasic solid–liquid. For all cosolvents, TBHP solutions, and reaction temperatures tested, the PXRD (Figure 7) and FT-IR ATR spectra (Figure S5, Supporting Information) of the solids recovered by centrifugation of the reaction mixtures after a 24 h batch run were similar to those of **1**. Hence, compound **1** seems to be fairly oxidatively and hydrolytically stable under the TBHP-based conditions. The poor catalytic performance may be partly due to the inability of **1** to activate TBHP for the catalytic reaction.

When aqueous H_2O_2 was used as oxidant instead of TBHP, the reaction of Cy in the presence of **1** was much faster, giving CyO as the only product in 77% yield at $55^\circ C/24$ h and 98% yield at $70^\circ C/24$ h, with CH_3CN as cosolvent (Figure 6, Table 4). No cocatalyst is necessary to obtain fairly good catalytic results for the system **1**/ H_2O_2 . For example, it has been reported for $[WO(O_2)(L)_2]$ ($L = N$ -cinnamyl- N -phenyl-hydroxamic acid), tested as catalyst in the same reaction, that no epoxidation reaction occurred without $NaHCO_3$ as cocatalyst (Table 5).³⁷ Another example of a tungsten-based (pre)catalyst that performs well for the epoxidation of Cy with aq H_2O_2 in the absence of a cocatalyst is the cyclopentadienyl oxotungsten(VI) complex $[Cp^*W_2O_5]$, which gave an epoxide yield of about 90% after ca. 100 min reaction at $55^\circ C$ (Table 5).³⁸ For compounds of the type $[Fe(L)(CH_3CN)_2](ClO_4)_2$ ($L =$ aminopyridine ligand), the epoxidation of Cy with H_2O_2 (CH_3CN as cosolvent) was much faster than that found for **1**, although in the former case a large excess of acetic acid was used to promote the catalytic reaction (Table 6).⁴² Complexes of the type $[ReO_3(CH_3)L]$ [$L =$ bis(fluorous-ponytailed)-2,2'-bipyridines] led to faster reaction of Cy than **1** at $55^\circ C$;

Table 5. Comparison of the Catalytic Results for **1** with Literature Data for Selected Tungsten Complexes Tested as Catalysts in the Reaction of *cis*-Cyclooctene with H₂O₂ or TBHP

(pre)catalyst	solvent/cocatalyst	reaction conditions ^a				conv ^b (%)	sel ^c (%)	ref
		T (°C)	[Cy] ₀ (M)	[W] ₀ (M)	t (h)			
H ₂ O ₂ as Oxidant								
1	EtOH/–	70	0.7	0.007	24	99	100	tw ^d
1	CH ₃ CN/–	55	0.7	0.007	24	77	100	tw
1	CH ₃ CN/–	70	0.7	0.007	24	98	100	tw
[WO(O ₂)(L) ₂] ^e	CH ₃ CN/–	25	0.83	~0.0004		~0	–	37
[WO(O ₂)(L) ₂] ^e	CH ₃ CN/NaHCO ₃	25	0.83	~0.0004	0.5	72	100	37
[Cp* ₂ W ₂ O ₅]	CH ₃ CN + toluene/–	55	0.27	0.0054	1.67	~90	100	38
TBHP as Oxidant								
1	–	55	2.4	0.024	4/24	2/10	100	–
1	–	70	2.4	0.024	4/24	13/57	100	–
[Cp* ₂ W ₂ O ₅]	CDCl ₃ /–	at	1.15	0.011	14 ^f	0.02	100	30
[Cp* ₂ W ₂ O ₅]	(CD ₃) ₂ CO/–	at	1.15	0.011	7 ^f	–	–	30
[Cp* ₂ W ₂ O ₅]	CH ₃ OD/–	at	1.15	0.011	6 ^f	–	–	30
[Cp* ₂ W ₂ O ₅]	CD ₃ CN/–	at	1.15	0.011	2 ^f	–	–	30
[Cp ^{ansa} W(CO) ₃]	–	55	2.03	0.020	4	<10	100	36
[CpW(CO) ₃ CH ₃]	–	55	2.03	0.020	4	<10	100	36

^aReaction conditions: T = reaction temperature (at = ambient temperature), [Cy]₀ = initial molar concentration of Cy, [W]₀ = initial molar concentration of W, t = reaction time. ^bConversion of Cy. ^cSelectivity toward CyO. ^dtw = This work. ^eL = *N*-cinnamyl-*N*-phenylhydroxamic acid. ^fReaction time in days.

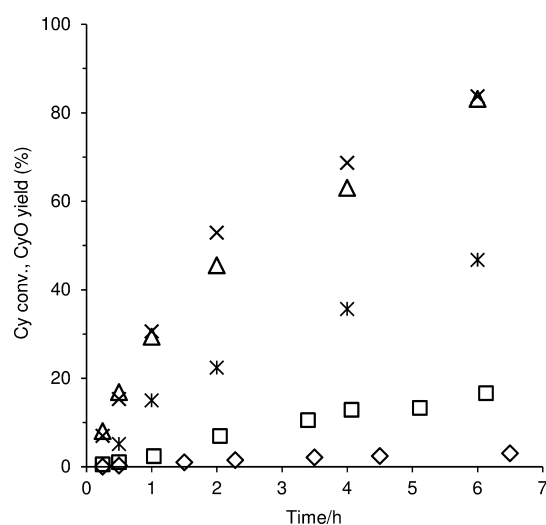


Figure 6. Dependence of Cy conversion and CyO yield on the time of reaction in the presence of **1** with TBHP_{dec}/ (no cosolvent) at 55 °C (◇) or 70 °C (□), H₂O₂/CH₃CN (*) at 55 °C, and H₂O₂/EtOH (Δ) or H₂O₂/CH₃CN (×) at 70 °C. For all catalytic tests, CyO selectivity was always 100%.

however, twice the molar amount of metal was used in the case of the rhenium catalysts, and halogenated cosolvents were used.⁴³

Iodometric titrations (ca. 10% error) for the systems **1**/H₂O₂/(EtOH or CH₃CN) heated at 70 °C for 24 h (without olefin) indicated no significant decomposition of the oxidant. These results suggest that, for **1**, H₂O₂ is productively consumed in the epoxidation process (i.e., negligible H₂O₂ decomposition to water plus molecular oxygen).

The catalytic results for **1**/H₂O₂ are far superior to those obtained for the molybdenum analogue [MoO₃(2,2'-bpy)], tested as catalyst under similar reaction conditions (Table 6): 83% and 25% conversion for **1** and [MoO₃(2,2'-bpy)], respectively, at 6 h reaction, with CyO as the only reaction

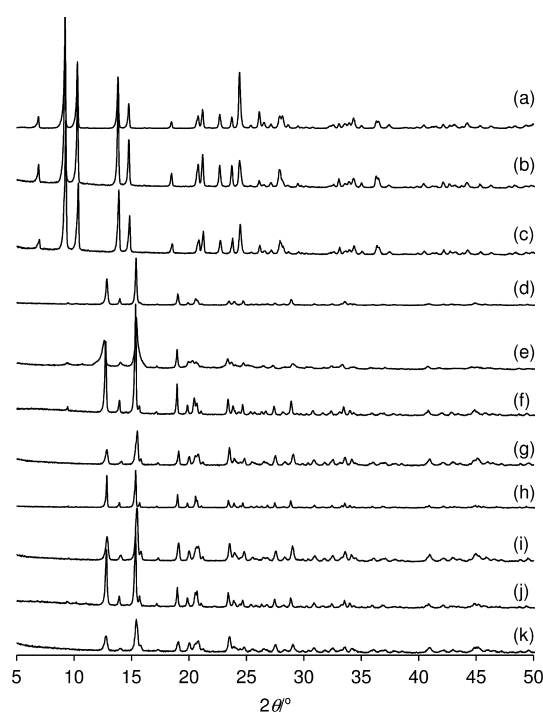


Figure 7. PXRD patterns of **1** (a) and the corresponding solid recovered from a 24 h batch run using TBHP_{dec}/EtOH (b), TBHP_{aq}/CH₃CN (c), H₂O₂/CH₃CN (d), and H₂O₂/EtOH [(**1**/H₂O₂/EtOH)-run1 (e), (**1**/H₂O₂/EtOH)-run 2 (f), (**1**/H₂O₂/EtOH)-run 3 (g)], at 70 °C. The remaining patterns are for the solids obtained from the contact tests, namely, sol-CT-CH₃CN (h) and sol-CT-EtOH (i), and the solids recovered from a batch run with sol-CT-CH₃CN and sol-CT-EtOH [(sol-CT-CH₃CN)-run1 (j) and (sol-CT-EtOH)-run1 (k), respectively].

product. Other related molybdenum(VI) compounds containing the 2,2'-bipyridine ligand, such as the hybrid material {[MoO₃(2,2'-bpy)][MoO₃(H₂O)]}_n²⁰ gave poorer results when tested as catalysts in the same reaction (Table 6). A

Table 6. Comparison of the Catalytic Results for 1 with Literature Data for Compounds Possessing Bipyridine-type Ligands, Tested as Catalysts in the Reaction of *cis*-Cyclooctene with H₂O₂^a

(pre)catalyst	reaction conditions						conv. (%)	sel. (%)	ref
	solvent	T (°C)	[Cy] ₀ (M)	[M] ₀ (M)	t (h)				
1	EtOH	70	0.7	0.007	6/24	83/99	100	tw	
1	CH ₃ CN	55	0.7	0.007	6/24	47/77	100	tw	
1	CH ₃ CN	70	0.7	0.007	6/24	84/98	100	tw	
2	CH ₃ CN	70	0.7	0.007	24	98	100	tw	
[MoO ₃ (2,2'-bpy)]	EtOH	70	0.7	0.007	6/24	25/71	100	tw	
{[MoO ₃ (2,2'-bpy)][MoO ₃ (H ₂ O)]} _n	CH ₂ Cl ₂	55	1.0	0.01	48	10	100	20	
[Mo(O ₂) ₂ (H ₂ O) _n] + 2eq 2,2'-bpy	CHCl ₃	60	0.1	0.0024	18	12	<1	39	
[MoO(O ₂) ₂ (2,2'-bpy)]	[C ₈ mim]PF ₆ ^b	60	0.45	0.011	18	61	38	40	
[MoO(O ₂) ₂ (2,2'-bpyO ₂) ^c	[C ₈ mim]PF ₆	60	0.45	0.011	18	65	100	40	
[MoO(O ₂) ₂ (2,2'-bpy)]	CH ₂ Cl ₂	at	1.22	0.0037	6	40	100	41	
[MoO(O ₂) ₂ (4,4'-bpy)]	CH ₂ Cl ₂	at	1.22	0.0037	6	30	100	41	
[Fe(L)(CH ₃ CN) ₂](ClO ₄) ₂ ^d	CH ₃ CN ^e	at	0.09	~0.0005	0.08	100	100	42	
[ReO ₃ (CH ₃)(2,2'-bpy)]	CH ₂ Cl ₂	at	0.1	0.002	5	>98	100	43	
[ReO ₃ (CH ₃)(bpy-F _n)] ^f	CH ₂ Cl ₂	at	0.1	0.002	5	>98	100	43	
[ReO ₃ (CH ₃)(4,4'-Me ₂ -2,2'-bpy)]	CH ₂ Cl ₂	25	0.88	0.0088	3	98	100	44	
[ReO ₃ (CH ₃)(2,2'-bpy)]	CH ₂ Cl ₂	at	0.95	0.0095	2/24	72/72	100	45	
[ReO ₃ (CH ₃)(Me ₂ -2,2'-bpy)]	CH ₂ Cl ₂	at	0.95	0.0095	1	~100	100	45	

^aSee footnotes a–d in Table 5 for abbreviations. ^b[C₈mim]PF₆ = 1-*n*-octyl-3-methylimidazolium hexafluorophosphate. ^c2,2'-bpyO₂ = 2,2'-bipyridine N,N'-dioxide. ^dL = bipyridine biperidine. ^eExcess acetic acid was used. ^fbpy-F_n = bis(fluorous-ponytailed) 2,2'-bipyridine with the substituent group (CH₂)₃(CF₂)₅CF₃.

similar trend has been reported for oxomolybdenum/tungsten analogues possessing cyclopentadienyl ligands, where the W compound was more effective than the Mo analogue for the catalytic epoxidation of olefins and oxidation of thiophenes with H₂O₂.^{30,38,46} A theoretical study (based on DFT calculations) by Dinoli et al. indicated a lower activation barrier for [Cp*₂W₂O₅] than for its Mo analogue, which is consistent with the higher catalytic activity of the former.³⁸ It has been proposed that the reaction mechanism for tungsten coordination compounds involves the primary activation of H₂O₂, where an oxo ligand (W=O) is protonated with concomitant formation of a hydroxide–hydroperoxo intermediate possessing the moiety {W(OH)(OαOβH)}, in which (OαOβH) is η²-coordinated; this intermediate plays a role in the oxygen atom transfer reaction to the olefin.³⁸ On the other hand, for the molybdenum-based catalytic system [Cp*MoO₂Cl]/H₂O₂, the active hydroperoxo intermediates formed may undergo isomerization (via proton transfer) to give less active peroxo derivatives.⁴⁷

Identification of Active Species and Catalytic Stability with H₂O₂. For the reaction systems 1/H₂O₂/(CH₃CN or EtOH), the mixtures were biphasic solid–liquid. The solids were recovered after a 24 h batch run [giving (1/H₂O₂/CH₃CN)-run1 and (1/H₂O₂/EtOH)-run1] and characterized by FT-IR ATR spectroscopy, PXRD, and SEM. These solids exhibited comparable PXRD patterns (Figure 7) and FT-IR ATR spectra (Figure 8), which are clearly different from those of 1. Hence, 1 is converted into different species under these reaction conditions. SEM revealed a change in morphology from thin, long needles for 1 to larger, irregular blocks for the recovered solids (Figure 2). The solid (1/H₂O₂/EtOH)-run1 was reused twice (with H₂O₂/EtOH, at 70 °C; details given in the Experimental Section). The catalytic results were similar for the three batch runs (Table 7). Moreover, the crystalline structures (Figure 7), FT-IR ATR spectra (Figure 8), and particle morphologies (Figure 2) of the solids recovered after each run were similar. To assess more closely the rate of

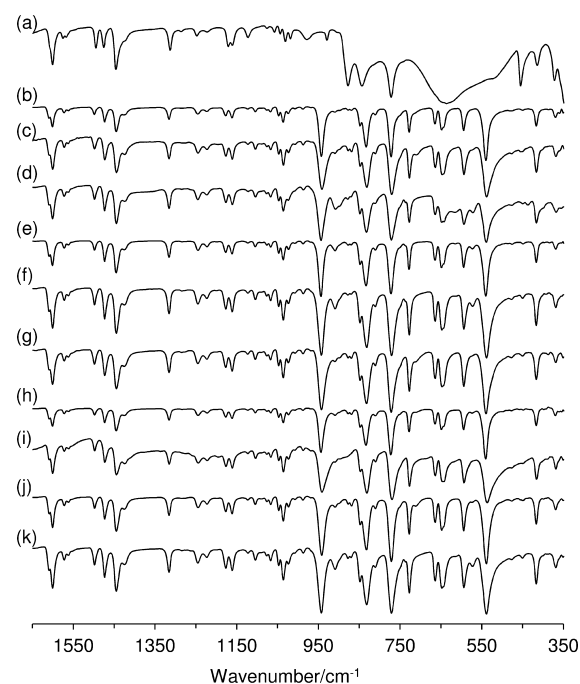


Figure 8. FT-IR ATR spectra of 1 (a) and the corresponding solids recovered from a 24 h batch run with aqueous H₂O₂ as oxidant and CH₃CN as cosolvent, at 55 °C (b) or 70 °C (c), and with EtOH as cosolvent at 70 °C [(1/H₂O₂/EtOH)-run1 (d), (1/H₂O₂/EtOH)-run 2 (e), (1/H₂O₂/EtOH)-run 3 (f)]. The remaining spectra are for the solids obtained from the contact tests, namely, sol-CT-CH₃CN (g) and sol-CT-EtOH (h), Prec-liq-CT-CH₃CN (i), and the solids recovered from a batch run with sol-CT-CH₃CN and sol-CT-EtOH [(sol-CT-CH₃CN)-run1 (j) and (sol-CT-EtOH)-run1 (k), respectively].

transformation of 1, additional reactions were performed for each cosolvent at 70 °C, and the solids present in the reaction mixtures were isolated after 15, 30, 60, and 120 min reaction

Table 7. Consecutive Batch Runs of Epoxidation of *cis*-Cyclooctene with H₂O₂ using 1 as Precatalyst and Catalytic Tests with Solid (sol) and Liquid (liq) Phases of the Contact Tests for 1 with EtOH and CH₃CN^a

sample	cosolvent	conversion (%)	CyO selectivity (%)
(1/H ₂ O ₂ /EtOH)-run1	EtOH	99	100
(1/H ₂ O ₂ /EtOH)-run2	EtOH	97	100
(1/H ₂ O ₂ /EtOH)-run3	EtOH	99	100
sol-CT-EtOH	EtOH	96	100
liq-CT-EtOH	EtOH	100	100
sol-CT-CH ₃ CN	CH ₃ CN	97	100
liq-CT-CH ₃ CN	CH ₃ CN	98	100

^aReaction conditions: initial molar ratios of W: Cy: oxidant = 1:100:167, 2 mL of cosolvent, 24 h, 70 °C.

times. With CH₃CN as cosolvent, the FT-IR spectrum of the solid after 15 min was similar to that of the solid recovered from a 24 h batch run [(1/H₂O₂/CH₃CN)-run1] (Figure S6 in the Supporting Information). On the other hand, with EtOH as cosolvent, the FT-IR spectrum of the solid after 15 min exhibited a mix of spectral features indicative of both 1 and (1/H₂O₂/EtOH)-run1, suggesting that the transformation of 1 is slower with this cosolvent than with CH₃CN. Nevertheless, after 1 h with EtOH as cosolvent, the transformation of 1 into the new species was evidently complete. Hence, 1 seems to be converted into a single, stable compound under the reaction conditions used.

In order to check for the catalytic contribution of (undissolved) metal species and their chemical nature, contact tests (CTs) were carried out for 1/H₂O₂ as described in the Experimental Section (without substrate, using EtOH or CH₃CN as cosolvent, at 70 °C). The resultant solids (denoted

sol-CT-EtOH and sol-CT-CH₃CN) and liquid phases (denoted liq-CT-EtOH and liq-CT-CH₃CN) were tested in the reaction of Cy with H₂O₂. Catalytic results for sol-CT and liq-CT (96–100% conversion at 24 h) were similar to those obtained for 1 (Tables 6 and 7). Hence, dissolved metal species play an important role, and the reaction of Cy occurs via homogeneous catalysis. Indeed, the solids sol-CT-EtOH and sol-CT-CH₃CN exhibited similar FT-IR spectral features (Figure 8) and crystalline structures (Figure 7), matching the data obtained for the solids recovered after 24 h batch catalytic runs. After using sol-CT-EtOH and sol-CT-CH₃CN in the catalytic tests, the resultant recovered solids [denoted (sol-CT-EtOH)-run1 and (sol-CT-CH₃CN)-run1] exhibited similar FT-IR spectral features and PXRD patterns to those displayed by sol-CT-EtOH and sol-CT-CH₃CN (Figures 7 and 8).

To check if the chemical nature of the dissolved metal species was similar to that of the undissolved compound (sol-CT-CH₃CN), attempts were made to isolate metal species from liq-CT-CH₃CN. This was successfully accomplished by adding *n*-hexane to the solution and leaving it overnight at 4 °C; the precipitated solid was separated by centrifugation (3500 rpm), washed with CH₃CN, and dried, giving a solid denoted as Prec-liq-CT-CH₃CN. The FT-IR spectral features of the solids Prec-liq-CT-CH₃CN and sol-CT-CH₃CN were very similar (Figure 8), supporting the above hypothesis that 1 is converted to a single, stable compound and that the latter is responsible for the observed homogeneous catalytic reaction. With the aim of unambiguously identifying this compound, a large-scale (33-fold increase) experiment was carried out for 1/H₂O₂/CH₃CN (without olefin; please see the Experimental Section for details). After 24 h of reaction at 70 °C, the reaction mixture was cooled to ambient temperature and filtered to isolate a

Table 8. Olefin Epoxidation with H₂O₂ in the Presence of 1 or 2, Using CH₃CN as Solvent^a

substrate	conv ^b (%)		epoxide sel ^c (%)		other reaction products ^d (%)	
	1	2	1	2	1	2
<i>cis</i> -cyclooctene	98	98	100	100	–	–
cyclododecene	83	79	100	100	–	–
<i>trans</i> -2-octene	92	93	64	79	2,3-octanediol 2-octene-4-one 3-octene-2-one (12) 3,4-epoxy-2-octanone (9) 3,5-octadiene-2-ol (6)	2,3-octanediol 2-octene-4-one 3-octene-2-one (6) 3,4-epoxy-2-octanone (5) 3,5-octadiene-2-ol (5)
1-octene	27	27	95	96	1,2-octanediol heptanal 2-octenal 1-octene-3-one heptanoic acid	1,2-octanediol heptanal 2-octenal 1-octene-3-one heptanoic acid
(<i>R</i>)-limonene	84	81	56 ^e	57 ^e	4-isopropenyl-1-methyl-1,2-cyclohexanediol (37) 5-isopropenyl-2-methyl-7-oxobicyclo[4.1.0]heptan-2-ol	4-isopropenyl-1-methyl-1,2-cyclohexanediol (36) 5-isopropenyl-2-methyl-7-oxobicyclo[4.1.0]heptan-2-ol
styrene	74	76	3	4	styrene glycol (17) benzaldehyde (43) benzoic acid (12) 2-hydroxyacetophenone (23) benzene acetaldehyde acetophenone	styrene glycol (10) benzaldehyde (44) benzoic acid (14) 2-hydroxyacetophenone (25) benzene acetaldehyde acetophenone

^aReaction conditions: initial molar ratios of W: Cy: oxidant = 1:100:167, 2 mL of cosolvent, 24 h, 70 °C. ^bOlefin conversion. ^cEpoxide product selectivity. ^dByproducts (results in parentheses are the selectivities for the main byproducts identified). ^eThe epoxide products were 1,2-epoxy-*p*-menth-8-ene and 1,2-8,9-diepoxy-*p*-menthane, and the molar ratio of 1,2-epoxy-*p*-menth-8-ene/1,2-8,9-diepoxy-*p*-menthane was 2.5 and 3.1 for 1 and 2, respectively.

colorless solid, which was identified as the oxodiperoxo complex $[\text{WO}(\text{O}_2)_2(2,2'\text{-bpy})]$ (**2**) by elemental analysis, single-crystal (see below) and powder XRD, FT-IR, and NMR spectroscopy. A comparison of the FT-IR spectral features of **2** with those for the recovered solids described above confirms that complex **2** is the catalytically active species formed from **1** in the presence of aqueous H_2O_2 . The FT-IR spectrum of **2** shows bands at 944 cm^{-1} [$\nu(\text{W}=\text{O})$]; 847 and 835 cm^{-1} [$\nu(\text{O}-\text{O})$]; and 649 , 595 , and 541 cm^{-1} [$\nu(\text{W}-\text{O})_{\text{peroxo}}$], which are all characteristic of $[\text{MO}(\text{O}_2)_2\text{L}]$ complexes bearing one bidentate ligand (L).^{16,21} The $^{13}\text{C}\{^1\text{H}\}$ CP MAS NMR spectrum of **2** displays 10 separate signals in the range of 120–155 ppm, indicating that the two pyridyl groups of the ligand are not equivalent in the crystal structure of **2** (Figure 3).

In consonance with that observed for **1**, the solid recovered after a catalytic run ($70\text{ }^\circ\text{C}$, 24 h) using $[\text{MoO}_3(2,2'\text{-bpy})]$ as precatalyst, 30% aq H_2O_2 as oxidant, and EtOH as cosolvent was identified by FT-IR and PXRD as the complex $[\text{MoO}(\text{O}_2)_2(2,2'\text{-bpy})]$. The recovered solid displayed bands in the FT-IR spectrum at 534 , 579 , and 648 cm^{-1} [$\nu(\text{Mo}-\text{O})_{\text{peroxo}}$]; 856 cm^{-1} [$\nu(\text{O}-\text{O})$]; and 935 cm^{-1} [$\nu(\text{Mo}=\text{O})$], in agreement with published data for the oxodiperoxo complex (Figure S7 in the Supporting Information).⁴⁸ As will be described below, the complexes $[\text{MO}(\text{O}_2)_2(2,2'\text{-bpy})]$ ($\text{M} = \text{Mo}, \text{W}$) are isotypical. Accordingly, the PXRD pattern for the recovered solid closely matched that for **2** (Figure S1, Supporting Information).

The solubility of **2** was apparently greater in CH_3CN than in EtOH since generally a lower amount of solid was recovered for the former. These observations are consistent with the faster conversion of **1** into **2** in CH_3CN discussed above (monitored by FT-IR). However, the kinetics of the epoxidation of Cy is roughly comparable for the two cosolvents. Possibly, the type of cosolvent influences the stability of transition states formed in the catalytic cycle.

The reaction of Cy with H_2O_2 , in the presence of **2** (CH_3CN as cosolvent), led to CyO as the only product formed with 98% yield at 24 h, $70\text{ }^\circ\text{C}$ (Table 6). These results are similar to those obtained for **1**. Hence, **1** is transformed in situ into **2**, which is responsible for the catalytic reaction. The catalytic results for **2** are far superior to those reported in the literature for the molybdenum analogue $[\text{MoO}(\text{O}_2)_2(2,2'\text{-bpy})]$ tested in the same reaction, under similar conditions (Table 6).^{40,41} This trend somewhat parallels that observed for **1** and its molybdenum analogue $[\text{MoO}_3(2,2'\text{-bpy})]$ (discussed above). The FT-IR spectrum of the solid recovered from the reaction of Cy in the presence of **2** was similar to that for the original complex (Figure S8, Supporting Information), suggesting that **2** is fairly stable.

Reactivity of Other Olefins in the Presence of **1** or **2**.

The catalytic performances of the two compounds were further investigated for the epoxidation of different olefins, namely, cyclododecene, *trans*-2-octene, 1-octene, styrene, and (*R*)-limonene, using H_2O_2 as oxidant and CH_3CN as cosolvent, at $70\text{ }^\circ\text{C}$, 24 h (Table 8). In general, with each substrate, **1** and **2** led to comparable conversions, similar to that observed with Cy as substrate. These results are consistent with the above hypothesis that **2** was responsible for the catalytic reaction.

The epoxide selectivity was excellent (100%) for the substrates Cy and cyclododecene, very high for 1-octene (87–95%), fair for *trans*-2-octene (64–79%) and (*R*)-limonene (56–57%), and very poor for styrene (3–4%). Some of the reaction byproducts identified by GC–MS are listed in Table 8. For the substrates 1-octene, *trans*-2-octene, (*R*)-limonene, and

styrene, the respective diol product (1,2-diol in the case of (*R*)-limonene) was formed, which most likely occurred via hydrolysis of the (relatively sensitive) epoxides. The poor epoxide selectivity in the reaction of styrene was accompanied by the formation of various byproducts, including 2-hydroxyacetophenone, benzaldehyde, and benzoic acid, suggesting that deeper oxidation occurred.

The results indicate that the cyclic olefin Cy is more reactive than cyclododecene, which may be due to steric effects associated with the epoxidation of the bulkier olefin. For the C8 linear olefins 1-octene and *trans*-2-octene, the more substituted olefin *trans*-2-octene is substantially more reactive than the terminal one. A similar reactivity trend was observed for the diene substrate (*R*)-limonene, for which selectivity to 1,2-epoxy-*p*-menth-8-ene was higher than that to 1,2-8,9-diepoxy-*p*-menthane. Hence, regioselectivity favored the epoxidation of the endocyclic C=C bond over the terminal one. These results suggest that the catalytic reactions may be governed by steric and/or electronic effects. The FT-IR ATR spectra of the solids recovered after using **1** or **2** with the different olefins were similar to that for **2** (Figure S8, Supporting Information), which is consistent with the catalyst stability of **2** discussed above.

Crystal Structure of $[\text{WO}(\text{O}_2)_2(2,2'\text{-bpy})]$ (2**).** The crystal structure of **2** is isotypical with that of the Mo^{VI} analogue published by Schlemper et al. in the early 1980s, as clearly depicted by the unit cell parameters and space group symmetry summarized in Table 2.⁴⁹ A search of the literature reveals, to the best of our knowledge, that this latter compound was the first reported oxodiperoxo Mo^{VI} compound. Compound **2** is, surprisingly, the first crystallographically determined structure of a compound of this kind based on W^{VI} centers. Since the report by Schlemper et al., over a dozen related structures (with Mo^{VI}) have been reported, most of them comprising *N,N'*-chelated organic linkers in the metal coordination sphere. Besides the recent work of Herbert et al. with 3-methylpyrazole and pyrazole,^{40,50} all remaining known structures are based on *N,N'*-chelated organic linkers.⁵¹

The asymmetric unit of compound **2** is composed of a whole molecular unit as depicted in Figure 9a. The crystallographically independent W^{VI} center is coordinated to two peroxy groups, one terminal oxo moiety, and, as in compound **1**, an *N,N'*-chelated 2,2'-bpy organic ligand. The W–(N,O) bond distances were found in the 1.726(5)–2.297(6) Å range (Table 9), with the shorter being attributed to the terminal oxo group and the longer ones to the connections to the organic ligand. The overall $\{\text{WN}_2\text{O}_3\}$ coordination sphere can be simplified by solely considering the centers of gravity of the two coordinated peroxy groups, leading to a distorted trigonal bipyramidal coordination environment, as depicted in Figure 9b. Table 9 summarizes the most relevant geometrical information concerning these two ways of considering the coordination environment of the W^{VI} centers in **2**.

Even though the $[\text{WO}(\text{O}_2)_2(2,2'\text{-bpy})]$ complex is rich in atoms capable of acting as strong acceptors in hydrogen-bonding interactions, the molecule only has these atoms bound to carbon, and therefore, only weak supramolecular interactions mediate the crystal packing of **2**. A series of weak C–H...O interactions (Table S2 in the Supporting Information) connect neighboring $[\text{WO}(\text{O}_2)_2(2,2'\text{-bpy})]$ complexes in the crystal structure, with the most important interactions being represented in Figure S9 (Supporting Information). The cooperative nature of these interactions, together with the

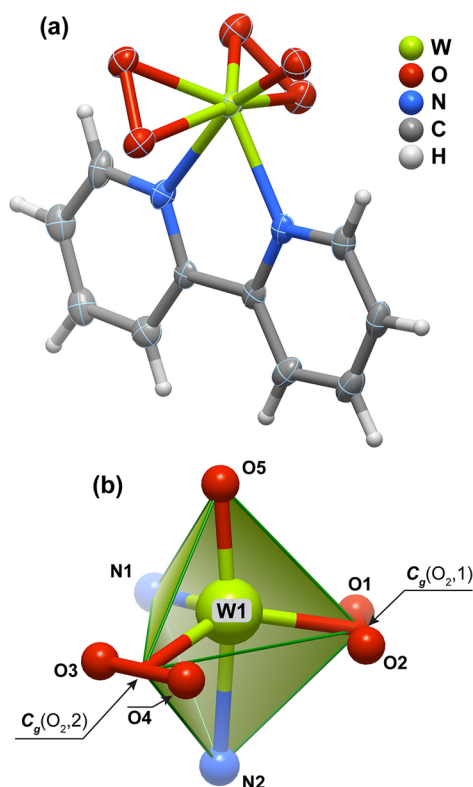


Figure 9. (a) Schematic representation of the discrete complex present in the asymmetric unit of compound $[\text{WO}(\text{O}_2)_2(2,2'\text{-bpy})]$ (**2**). Non-hydrogen atoms are represented as thermal ellipsoids drawn at the 50% probability level and hydrogen atoms as small spheres with arbitrary radii. (b) Simplified polyhedral representation of the W^{VI} coordination environment, evidencing the distorted trigonal bipyramidal coordination environment when the centers of gravity of the peroxo groups are taken as the central coordination site. Selected bond lengths and angles are given in Table 8

fact that most are relatively directional [interaction $\angle(\text{DHA})$ angles typically above ca. 150°] and with short $\text{D}\cdots\text{A}$ distances (see Table S2, Supporting Information), boosts their importance in the crystal packing of **2**. On the other hand, the coordinated 2,2'-bpy ligands are also engaged in a series of $\pi\cdots\pi$ stacking interactions, as depicted in Figure S10 of the Supporting Information (for geometrical data, see Table S2, Supporting Information). A view of the crystal packing is given in Figure S11 (Supporting Information).

CONCLUSIONS

A new structural variant of a tungsten oxide/2,2'-bipyridine hybrid material with the composition $[\text{WO}_3(2,2'\text{-bpy})]\cdot n\text{H}_2\text{O}$ has been prepared and characterized. The use of a dynamic hydrothermal synthesis appears to be responsible for the formation of the unique crystal structure in **1**, which is composed of $\infty^1[\text{WO}_3(2,2'\text{-bpy})]$ polymeric chains in which the 2,2'-bpy ligands are located alternately above and below the growth axis of the chain rather than just on one side, as is found in the previously reported anhydrous phases $[\text{MO}_3(2,2'\text{-bpy})]$ ($\text{M} = \text{Mo}, \text{W}$), which were isolated after static hydrothermal syntheses. The catalytic behavior of **1** has been studied in detail for the epoxidation of the model substrate *cis*-cyclooctene. When aqueous H_2O_2 is used as the oxidant, **1** is quickly converted to the partially soluble oxodiperoxo complex $[\text{WO}(\text{O}_2)_2(2,2'\text{-bpy})]$ (**2**), which is the active species responsible for the selective epoxidation reaction in the homogeneous phase. Hence, for this particular reaction, compound **1** is useful as a stable and easily and safely storable catalyst precursor. Compounds **1** and **2** promoted the reaction of different olefins (cyclododecene, *trans*-2-octene, 1-octene, styrene, and (*R*)-limonene) using H_2O_2 as oxidant; with each olefin, the two compounds led to similar catalytic results. When compared with molybdenum, tungsten oxide/organonitrogen hybrid materials have been less well studied, with unsubstituted pyridine and bipyridine molecules being the most common ligands employed. Work is ongoing in our laboratory to expand

Table 9. Selected Bond Lengths (in Å) and Angles (in deg) for the Crystallographically Independent W^{VI} Metal Center Present in Compound $[\text{WO}(\text{O}_2)_2(2,2'\text{-bpy})]$ (**2**)^a

W1–O1	1.964(5)	W1–N1	2.180(6)
W1–O2	1.916(5)	W1–N2	2.297(6)
W1–O3	1.909(5)		
W1–O4	1.953(5)	W1– $\text{C}_g(\text{O}_2,1)$	1.792(3)
W1–O5	1.726(5)	W1– $\text{C}_g(\text{O}_2,2)$	1.783(3)
O1–W1–N1	86.1(2)	O4–W1–O1	157.2(2)
O1–W1–N2	78.6(2)	O4–W1–N1	86.4(2)
O2–W1–O1	45.3(2)	O4–W1–N2	78.6(2)
O2–W1–O4	133.0(2)	O5–W1–O1	100.0(2)
O2–W1–N1	130.2(2)	O5–W1–O2	104.7(2)
O2–W1–N2	86.4(2)	O5–W1–O3	106.5(2)
O3–W1–O1	132.8(2)	O5–W1–O4	101.8(2)
O3–W1–O2	89.9(2)	O5–W1–N1	91.8(2)
O3–W1–O4	45.1(2)	O5–W1–N2	163.1(2)
O3–W1–N1	130.2(2)	N1–W1–N2	71.3(2)
O3–W1–N2	85.9(2)		
$\text{C}_g(\text{O}_2,1)$ –W1– $\text{C}_g(\text{O}_2,2)$	132.51(2)	$\text{C}_g(\text{O}_2,2)$ –W1–O5	105.29(2)
$\text{C}_g(\text{O}_2,1)$ –W1–O5	103.38(2)	$\text{C}_g(\text{O}_2,2)$ –W1–N1	108.13(2)
$\text{C}_g(\text{O}_2,1)$ –W1–N1	107.93(2)	$\text{C}_g(\text{O}_2,2)$ –W1–N2	81.56(2)
$\text{C}_g(\text{O}_2,1)$ –W1–N2	81.83(2)		

^a $\text{C}_g(\text{O}_2,1)$: Center of gravity of the O1–O2 coordinated peroxo group. $\text{C}_g(\text{O}_2,2)$: Center of gravity of the O3–O4 coordinated peroxo group.

the structural diversity and catalytic potential of tungsten oxide/organic hybrid materials by using other bipyridine derivatives or related organonitrogen compounds as ligands for the metal oxide substructure.

■ ASSOCIATED CONTENT

■ Supporting Information

Detailed description of X-ray diffraction studies, Figures S1–S11, Tables S1 and S2, and crystallographic data in CIF format for compounds **1** and **2**. The Supporting Information is available free of charge on the ACS Publications website at DOI: 10.1021/acs.inorgchem.5b00928. Crystallographic data for compounds **1** and **2** reported in this Article have been deposited at the Cambridge Crystallographic Data Centre as CCDC 1054220 and 1054221, respectively. These data can be obtained free of charge from the Cambridge Crystallographic Data Centre via www.ccdc.cam.ac.uk/conts/retrieving.html.

■ AUTHOR INFORMATION

Corresponding Authors

*A.A.V. e-mail: atav@ua.pt.

*F.A.A.P. e-mail: filipe.paz@ua.pt.

*I.S.G. e-mail: igoncalves@ua.pt.

Notes

The authors declare no competing financial interest.

■ ACKNOWLEDGMENTS

We acknowledge funding by FEDER (Fundo Europeu de Desenvolvimento Regional) through COMPETE (Programa Operacional Factores de Competitividade). National funding through the FCT (Fundação para a Ciência e a Tecnologia) within the projects FCOMP-01-0124-FEDER-029779 (FCT ref PTDC/QEQ-SUP/1906/2012) and FCOMP-01-0124-FEDER-041282 (FCT ref EXPL/CTM-NAN/0013/2013) is thanked. This work was developed in the scope of the project CICECO—Aveiro Institute of Materials (FCT ref UID/CTM/50011/2013), financed by national funds through the FCT/MEC and cofinanced by FEDER under the PT2020 Partnership Agreement. The FCT and the European Union are acknowledged for postdoctoral grants to T.R.A. (SFRH/BPD/97660/2013) and M.M.A. (SFRH/BPD/89068/2012) cofunded by MCTES and the European Social Fund through the program POPH of QREN. The FCT and CICECO are acknowledged for financial support toward the purchase of the single-crystal diffractometer. The authors are grateful to the ESRF (Grenoble, France) for approving the experiment CH-4254.

■ REFERENCES

- (1) Hagrman, P. J.; Hagrman, D.; Zubieta, J. *Angew. Chem., Int. Ed.* **1999**, *38*, 2638–2684.
- (2) Hagrman, D.; Hagrman, P. J.; Zubieta, J. *Comments Inorg. Chem.* **1999**, *21*, 225–261.
- (3) Hagrman, P. J.; Finn, R. C.; Zubieta, J. *Solid State Sci.* **2001**, *3*, 745–774.
- (4) Johnson, J. W.; Jacobson, A. J.; Rich, S. M.; Brody, J. F. *J. Am. Chem. Soc.* **1981**, *103*, 5246–5247.
- (5) Hagrman, P. J.; LaDuca, R. L., Jr.; Koo, H.-J.; Rarig, R., Jr.; Haushalter, R. C.; Whangbo, M.-H.; Zubieta, J. *Inorg. Chem.* **2000**, *39*, 4311–4317.
- (6) Xu, Y.; Lu, J.; Goh, N. K. *J. Mater. Chem.* **1999**, *9*, 1599–1602.
- (7) Yan, B.; Xu, Y.; Goh, N. K.; Chia, L. S. *Chem. Commun.* **2000**, 2169–2170.

- (8) Zhang, X.; Hejazi, M.; Thiagarajan, S. J.; Woerner, W. R.; Banerjee, D.; Emge, T. J.; Xu, W.; Teat, S. J.; Gong, Q.; Safari, A.; Yang, R.; Parise, J. B.; Li, J. *J. Am. Chem. Soc.* **2013**, *135*, 17401–17407.
- (9) Zapf, P. J.; Haushalter, R. C.; Zubieta, J. *Chem. Mater.* **1997**, *9*, 2019–2024.
- (10) Twu, J.; Fang, T.-H.; Hsu, C.-F.; Yu, Y.-Y.; Wang, G.-J.; Tang, C.-W.; Chen, K.-H.; Lii, K.-H. *J. Mater. Chem.* **1998**, *8*, 2181–2184.
- (11) Lu, Y.; Wang, E.; Yuan, M.; Li, Y.; Hu, C. *J. Mol. Struct.* **2003**, *649*, 191–195.
- (12) Kim, J.; Lim, W. T.; Koo, B. K. *Inorg. Chim. Acta* **2007**, *360*, 2187–2191.
- (13) Amarante, T. R.; Neves, P.; Valente, A. A.; Paz, F. A. A.; Fitch, A. N.; Pillinger, M.; Gonçalves, I. S. *Inorg. Chem.* **2013**, *52*, 4618–4628.
- (14) Cui, C.-P.; Dai, J.-C.; Du, W.-X.; Fu, Z.-Y.; Hu, S.-M.; Wu, L.-M.; Wu, X.-T. *Polyhedron* **2002**, *21*, 175–179.
- (15) Zhou, Y.; Zhang, L.; Fun, H.-K.; You, X. *Inorg. Chem. Commun.* **2000**, *3*, 114–116.
- (16) Amarante, T. R.; Neves, P.; Gomes, A. C.; Nolasco, M. M.; Ribeiro-Claro, P.; Coelho, A. C.; Valente, A. A.; Paz, F. A. A.; Smeets, S.; McCusker, L. B.; Pillinger, M.; Gonçalves, I. S. *Inorg. Chem.* **2014**, *53*, 2652–2665.
- (17) Zapf, P. J.; LaDuca, R. L., Jr.; Rarig, R. S., Jr.; Johnson, K. M., III; Zubieta, J. *Inorg. Chem.* **1998**, *37*, 3411–3414.
- (18) Chuang, J.; Ouellette, W.; Zubieta, J. *Inorg. Chim. Acta* **2008**, *361*, 2357–2364.
- (19) Lysenko, A. B.; Senchyk, G. A.; Lincke, J.; Lässig, D.; Fokin, A. A.; Butova, E. D.; Schreiner, P. R.; Krautscheid, H.; Domasevitch, K. V. *Dalton Trans.* **2010**, *39*, 4223–4231.
- (20) Abrantes, M.; Amarante, T. R.; Antunes, M. M.; Gago, S.; Paz, F. A. A.; Margiolaki, I.; Rodrigues, A. E.; Pillinger, M.; Valente, A. A.; Gonçalves, I. S. *Inorg. Chem.* **2010**, *49*, 6865–6873.
- (21) Amarante, T. R.; Neves, P.; Paz, F. A. A.; Valente, A. A.; Pillinger, M.; Gonçalves, I. S. *Dalton Trans.* **2014**, *43*, 6059–6069.
- (22) Abrantes, M.; Gonçalves, I. S.; Pillinger, M.; Vurchio, C.; Cordero, F. M.; Brandi, A. *Tetrahedron Lett.* **2011**, *52*, 7079.
- (23) Udin, I.; Fox, M. R.; Martin, H.; Gainsford, G. J.; Kennedy, J.; Markwitz, A.; Telfer, S. G.; Jameson, G. B.; Tallon, J. L. *Chem. Commun.* **2010**, *46*, 4261–4263.
- (24) Chong, S. V.; Tallon, J. L. *J. Phys. Chem. Solids* **2010**, *71*, 303–308.
- (25) Udin, I.; Chong, S. V.; Telfer, S. G.; Kennedy, J.; Jameson, G. B.; Waterland, M. R.; Tallon, J. L. *J. Phys. Chem. C* **2012**, *116*, 3787–3792.
- (26) Amini, M.; Haghdoost, M. M.; Bagherzadeh, M. *Coord. Chem. Rev.* **2014**, *268*, 83–100.
- (27) Jørgensen, K. A. *Chem. Rev.* **1989**, *89*, 431–458.
- (28) Jimtaisong, A.; Luck, R. L. *Inorg. Chem.* **2006**, *45*, 10391–10402.
- (29) Tang, J.; Wang, L.; Liu, G.; Liu, Y.; Hou, Y.; Zhang, W.; Jia, M.; Thiel, W. R. *J. Mol. Catal. A: Chem.* **2009**, *313*, 31–37.
- (30) Sözen-Aktaş, P.; Manoury, E.; Demirhan, F.; Polı, R. *Eur. J. Inorg. Chem.* **2013**, 2728–2735.
- (31) Amarante, T. R.; Neves, P.; Coelho, A. C.; Gago, S.; Valente, A. A.; Paz, F. A. A.; Pillinger, M.; Gonçalves, I. S. *Organometallics* **2010**, *29*, 883–892.
- (32) Yan, B.; Xu, Y.; Goh, N. K.; Chia, L. S. *Inorg. Chem. Commun.* **2000**, *3*, 379–382.
- (33) Brandenburg, K. *DIAMOND, Version 3.2f*; Crystal Impact GbR: Bonn, Germany, 1997–2010.
- (34) Yang, S. H.; Li, G. B.; Tian, S. J.; Liao, F. H.; Lin, J. H. *Cryst. Growth Des.* **2007**, *7*, 1246–1250.
- (35) Baur, W. H. *Acta Crystallogr., Sect. B* **1974**, *30*, 1195–1215.
- (36) Zhao, J.; Santos, A. M.; Herdtweck, E.; Kühn, F. E. *J. Mol. Catal. A: Chem.* **2004**, *222*, 265–271.
- (37) Maiti, S. K.; Dinda, S.; Banerjee, S.; Mukherjee, A. K.; Bhattacharyya, R. *Eur. J. Inorg. Chem.* **2008**, 2038–2051.
- (38) Dinoi, C.; Ciclosi, M.; Manoury, E.; Maron, L.; Perrin, L.; Poli, R. *Chem.—Eur. J.* **2010**, *16*, 9572–9584.
- (39) Herbert, M.; Montilla, F.; Galindo, A. *J. Mol. Catal. A: Chem.* **2011**, *338*, 111–120.

- (40) Herbert, M.; Montilla, F.; Galindo, A.; Moyano, R.; Pastor, A.; Alvarez, E. *Dalton Trans.* **2011**, *40*, 5210–5219.
- (41) Afsharpour, M.; Mahjoub, A. R.; Amini, M. M. *Appl. Catal. A: Chem.* **2007**, *327*, 205–210.
- (42) Mikhalyova, E. A.; Makhlynets, O. V.; Palluccio, T. D.; Filatov, A. S.; Rybak-Akimova, E. V. *Chem. Commun.* **2011**, *48*, 687–689.
- (43) Saladino, R.; Ginnasi, M. C.; Collalto, D.; Bernini, R.; Crestini, C. *Adv. Synth. Catal.* **2010**, *352*, 1284–1290.
- (44) Altmann, P.; Kühn, F. E. *J. Organomet. Chem.* **2009**, *694*, 4032–4035.
- (45) Zhou, M.-D.; Jain, K. R.; Günyar, A.; Baxter, P. N. W.; Herdtweck, E.; Kühn, F. E. *Eur. J. Inorg. Chem.* **2009**, 2907–2914.
- (46) Ciclosi, M.; Dinoi, C.; Gonsalvi, L.; Peruzzini, M.; Manoury, E.; Poli, R. *Organometallics* **2008**, *27*, 2281–2286.
- (47) Comas-Vives, A.; Lledós, A.; Poli, R. *Chem.—Eur. J.* **2010**, *16*, 2147–2158.
- (48) Gamelas, C. A.; Gomes, A. C.; Bruno, S. M.; Paz, F. A. A.; Valente, A. A.; Pillinger, M.; Romão, C. C.; Gonçalves, I. S. *Dalton Trans.* **2012**, *41*, 3474–3484.
- (49) Schlemper, E. O.; Schrauzer, G. N.; Hughes, L. A. *Polyhedron* **1984**, *3*, 377–380.
- (50) Herbert, M.; Alvarez, E.; Cole-Hamilton, D. J.; Montilla, F.; Galindo, A. *Chem. Commun.* **2010**, *46*, 5933–5935.
- (51) (a) Figueiredo, S.; Gomes, A. C.; Fernandes, J. A.; Paz, F. A. A.; Lopes, A. D.; Lourenço, J. P.; Pillinger, M.; Gonçalves, I. S. *J. Organomet. Chem.* **2013**, *723*, 56–64. (b) Amarante, T. R.; Paz, F. A. A.; Gago, S.; Gonçalves, I. S.; Pillinger, M.; Rodrigues, A. E.; Abrantes, M. *Molecules* **2009**, *14*, 3610–3620. (c) Carreiro, E. D.; Yong-En, G.; Burke, A. J. *Inorg. Chim. Acta* **2006**, *359*, 1519–1523. (d) Brito, J. A.; Gómez, M.; Muller, G.; Teruel, H.; Clinet, J. C.; Duñach, E.; Maestro, M. A. *Eur. J. Inorg. Chem.* **2004**, 4278–4285. (e) Hinner, M. J.; Grosche, M.; Herdtweck, E.; Thiel, W. R. *Z. Anorg. Allg. Chem.* **2003**, *629*, 2251–2257. (f) Glas, H.; Spiegler, M.; Thiel, W. R. *Eur. J. Inorg. Chem.* **1998**, 275–281. (g) Thiel, W. R.; Priermeier, T. *Angew. Chem., Int. Ed. Engl.* **1995**, *34*, 1737–1738. (h) Thiel, W. R.; Angstl, M.; Priermeier, T. *Chem. Ber.* **1994**, *127*, 2373–2379. (i) Herrmann, W. A.; Thiel, W. R.; Kuchler, J. G.; Behm, J.; Herdtweck, E. *Chem. Ber.* **1990**, *123*, 1963–1970.